RESEARCHERID
THOMSON REUTERS

[Djanna Koffi* *et al.*, 6(9): September, 2017]
IC™ Value: 3.00

ISSN: 2277-9655
Impact Factor: 4.116
CODEN: IJESS7

IJESRT

INTERNATIONAL JOURNAL OF ENGINEERING SCIENCES & RESEARCH TECHNOLOGY

AN EXPERIMENTAL STUDY OF TURBULENT NATURAL CONVECTION IN AN AIR FILLED DIFFERENTIALLY HEATED CAVITY: THE TURBULENCE QUANTITIES

Djanna Koffi F.L. [*1,3], Tamba J. G. [1], Mtopi Fotso B. E. [2], Saury D. [3], Joubert P. [3], Lemmonier D.[3]

[1*] Department of Thermal Engineering, University Institute of Technology of Douala, Cameroon

[2] Laboratory of Engineering for Industrial Systems and Environment – LISIE, Department of Mechanical Engineering and Computed Integrated Manufacturing, FOTSO Victor Institute of Technology of Bandjoun, Cameroon

[3] Institut Pprime - UPR 3346, CNRS - ENSMA - Université de Poitiers, France.

DOI: Will get Assigned by IJESRT Team

ABSTRACT

An experimental study of high level turbulence natural convection in a 4m-height differentially heated cavity was conducted at large Rayleigh numbers ($4.0\times10^{10}\leq Ra_H\leq1.2\times10^{11}$). In this study, turbulence quantities including θ_{RMS} (θ'), V_{RMS} (V'), W_{RMS} (W'), turbulent kinetic energy (k) are presented. The power spectral densities show a characteristics frequency of about 0.046 Hz in the core region indicating the existence of internal waves. In the boundary layer, we recorded higher frequency up to 4.5 Hz along the fluid flow. Periodic oscillations in the form of Tollmien-Schlichting waves are found in the boundary layer, near the isothermal walls (from the wall to about 7 mm). The results indicate that the decay of spectrum follows an f^{-3} law in the boundary layer. Large-scale vortex structures are identified mainly on the edge of the hot boundary layer.

KEYWORDS: differentially heated cavity, natural convection, turbulence, turbulent kinetic energy, Tollmien-Schlichting instabilities.

I. INTRODUCTION

Due to its many engineering applications, turbulent natural convection arising in the vertical cavities with two differentially heated side walls has been an attractive subject in fundamental turbulence research. The cooling of electronic devices, solar energy collectors and air flow in buildings, for example can be simplified to this configuration. However, this type of flow is one of the most complicated fluid dynamic problems for several reasons: first of all, due to the interaction between the boundary layer and the core region, neither the flow in the boundary layer nor the flow in the core region can be determined by the boundary conditions alone; In addition, flow in vertical cavity can include simultaneously laminar, transitional and turbulent regions when the Rayleigh number exceeds a critical value; lastly, the buoyancy is the only driving force for fluid motion and imposes significant effects on the turbulence evolution in the near-wall boundary layer.

The mean temperature and the velocity profiles including global flow circulation in the upper part of the cavity was presented in [1]. In addition, the velocity maximum correlation as a function of the local Rayleigh number has been derived. The work presented in [1] included local and heat transfer along the isothermal walls. Thanks to the results from the present work, added with earlier reports, a complete correlation for the Nusselt number over a wide range of Rayleigh numbers has been provide [2].

This work is mainly focused on some turbulence fluid flow and thermal parameters, such as θ_{RMS} (θ'), V_{RMS} (V'), W_{RMS} (W'), turbulent kinetic energy (k), turbulence intensity (I), in order to determine the level of the turbulence flow in the cavity and to identify the type of instability in such configurations. Temperature and velocity measurements are not made simultaneously; then we are not able to record the Reynolds shear stress and the turbulent heat flux. Therefore direct measurement of these quantities, although very difficult, is highly desirable. The both terms are needed for example, in the governing equations to describe turbulent natural convection. It is as well as an experimental investigation is currently under way in the laboratory in order to estimate the Reynolds shear stress and the turbulent heat flux.

Up to now, very limited experimental turbulence data were reported. Giel and Schmidt [3] reported W′ and θ′ results in a water filled high cavity (A_V =10). Cheesewright and co-workers [4-6] built up a set of results including V′, W′, θ′, $\overline{V'W'}$, $\overline{V'\theta'}$, and $\overline{W'\theta'}$ for a cavity with A_V =5. They used the measured mean values to calculate the Reynolds stress. Betts and co-workers [7-8] measured V′ and W′ for a tall cavity (A_V =28.68). Lankhorst [9-10] gave some W′ results for a thin square cavity (A_H = 0.1). Mergui et al. [11] presented values of V′, W′, θ′, and $\overline{V'W'}$ for a shallow thin cavity (A_V =0.9, A_H =0.3). Tian and Kariayannis [12-14] reported a set of results including V′, W′, θ′, $\overline{V'W'}$ for an air filled square cavity at a Rayleigh number of 1.5×10^9. The results mentioned above featured strong asymmetry due to either heat losses [4-6] or limited aspect ratio in the depth direction [9,11]. Flow in cavities gets more confined near the wall as the Rayleigh number increases.

This paper is arranged as follows. In the next section, we describe experimental setup. Then, in the last two sections we present and discuss the experimental results of turbulent quantities respectively for the velocity field and temperature field.

All content should be written in English and should be in 1 column.

- Page type will be A4 with normal margin, word spacing should be 1.
- No space will be added before or after paragraph.
- This section should be typed in character size 10pt Times New Roman, Justified.

II. EXPERIMENTAL SETUP

A detailed description of the cavity, the experimental facility, the instrumentation and the procedure used was given in [1], it will not be repeated here. A 3D schematic of the cavity is included in this paper (**Fig. 1).** The test cell is a differentially heated cavity of 3.84 m high, 1 m wide and 0.86 m deep. Two opposite vertical walls are differentially heated. The main components of the experimental system, shown in **Fig. 2**, include the test cell, filled with air at atmospheric pressure, the 2D-PIV system, the facilities of measuring the temperature control system and the air temperature.

We just give in this paper some details about the accuracy of the instruments used and their ability to record turbulent quantities as fluctuation velocity and temperature.

Figure 1 :

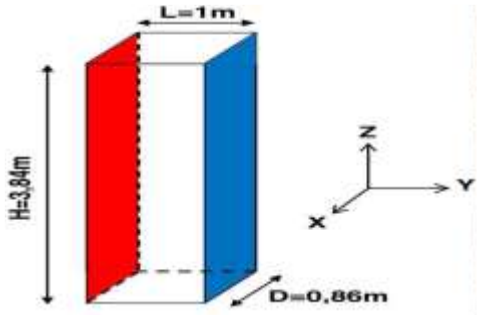

Scheme of the cavity

The thickness of the light-sheet, an important parameter in PIV, is readily adjustable, to 1mm. For this study a 12 bit Kodak Megaplus ES 1:0 with 1344 ×1024 pixels CCD camera was used to capture the images. To detect the position of the illuminated seeding particles, the CCD (Charge Coupled Device) camera is positioned at right angles to the light-sheet, and particle positions will appear as light specks on a dark background on each camera frame. The camera is located to 1.5 m in front of the visualization window (**Fig. 2**). The pulsing light-sheet and the camera are synchronized so that particle positions at the instant of light pulse number 1 are registered on frame 1 of the camera, and particle positions from pulse number 2 are on frame 2. The laser sends two pulses with a shorter time interval (from 10^{-3}s for ΔT=20K to 10^{-2}s for ΔT=7K) to the seeding particles. The frequency of the laser pulsation is of 4 Hz. Under these assumptions, we obtain 4 double Image per second (mean 2×4 images) in which 4 instantaneous velocity field are deducted. Otherwise, for each measurement we should put the window visualization to location we need to investigate and then ajust the camera with a displacement system programmable (*CharlyRobot)* with a very good accuracy (better than 0.1 mm). After all of these settings, it then starts the acquisition of 4 sets of measures each with 280 pictures (70s for each set). This value corresponds to the limit memory of camera used. Data analysis of the PIV was performed using the software package ‘‘Dynamic Studio”, described in detail in Dantec Dynamics [15].Subheading should be 10pt Times new Roman, justified.

ISSN: 2277-9655
Impact Factor: 4.116
CODEN: IJESS7

Figure 2 :

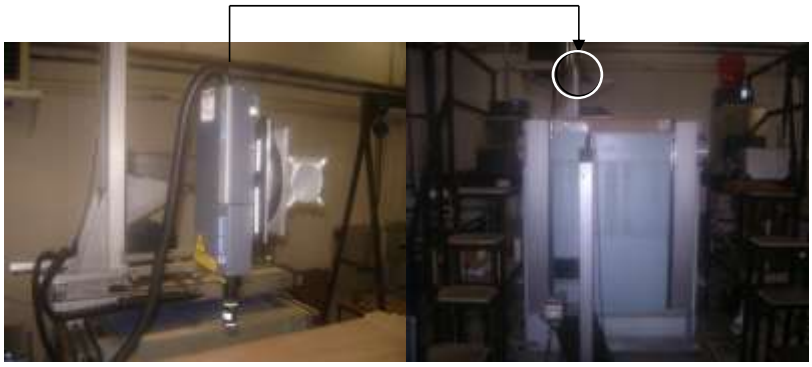

Photography of the experimental cavity and its measurement equipment

Temperature measurements in the cavity are carried out using a K-type micro-thermocouple of diameter 12.7 µm manufactured in situ, assembled on a vertical cane interdependent (**Fig. 3**) of a system of displacement motorized and controlled by computer. The displacement device was calibrated so that the accuracy of the thermocouple location was better than 0.2 mm. The micro-thermocouple is connected in opposition with a reference thermocouple (PT100) which located in its immediate vicinity. The terminal voltage of the micro-thermocouple is measured and recorded using a nano-voltmeter AGILENT 34420A, higher sensitivity multimeter with 1NPLC and $7^{1/2}$ digits resolution. 1024 readings were taken for each measurement. The temperature was read by a 18 bits data logging card (National Instrument PCI-6128 M Series). For every location, the measurement was made at least twice. If the difference between two measurements was less than 0.1 K, the second measurement was accepted and recorded. Finally, the local temperature is obtained with an accuracy of 0.1 K. The average and the root mean square (rms) of the fluctuation temperature were recorded.

A particular regard is laid on the follow-up of the experimental conditions, thus the temperature of control (heated and cooled walls temperatures, room temperature), the atmospheric pressure, the relative humidity are carried out and recorded continuously.

III. RESULTS AND DISCUSSION

III.1 Turbulent fluid flow parameters for $Ra_H = 1.2\times10^{11}$

III.1.1. The root mean square of the velocity fluctuation

- Vertical component

A mapping of the dimensionless vertical velocity component W and its RMS fluctuation associated W_{RMS} (or W') are reported in **Fig. 3**. There, we can clearly identify a flow boundary layer along the isothermal walls. We can note that the vertical velocity fluctuation is concentrated in the boundary layers and decrease to almost nothing outside the boundary layers. The vertical component of the dimensionless mean velocity and his rms fluctuation for different heights in the boundary layers are shown (**Fig. 4**).

As seen in **Fig. 4a**, the velocity reaches its maximum value of 0.12 in the hot boundary layer at the height Z=0.65. In this boundary layer (to the location Z=0.70), the measured maximum of the vertical velocity fluctuation is about 0.035, which corresponds to 29% of the maximum mean velocity recorded in the cavity. It can be seen from **Fig. 4b** that vertical velocity fluctuation remains relatively high into the viscous layer next to the isothermal hot wall. We also observe that, between the buoyant sub-layer and the outer edge of the hot boundary layer, the distribution of the fluctuations describes a "bearing" indicating that, for each given height, the fluctuations seem to be almost constant in this turbulent area. This trend was already observed in the past by Salat [16], with a Rayleigh number of 1.5×10^{9}.

- Horizontal component

A mapping of the dimensionless horizontal velocity component V and its RMS fluctuation associated V_{RMS} (or V') are reported in **Fig. 5.** The horizontal fluctuations remain significant in the hot boundary layer (to the location $0.65 \leq Z \leq 0.75$), reaching 0.021 (**Fig. 6a**), which corresponds to 17% of the maximum mean velocity recorded. This region where found the maximum of vertical and horizontal velocity fluctuations, seems to be characterized by a fully developed turbulence.

Examination of **Fig. 6b** reveals an increase of horizontal velocity fluctuations in the cold boundary layer ($0.65 \leq Z \leq 0.75$), due probably to the fact that the cold boundary layer is simultaneously fed by the fluid from the main the secondary flow near the ceiling and the hot boundary layer.

ISSN: 2277-9655
Impact Factor: 4.116
CODEN: IJESS7

Figure 3 :

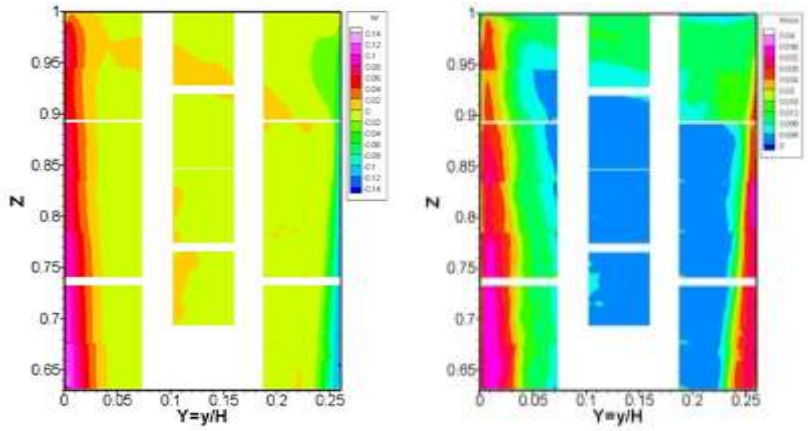

Mapping of vertical component of the dimensionless mean velocity and its RMS fluctuation for Ra_H =1,2×10^{11}

Figure 4 :

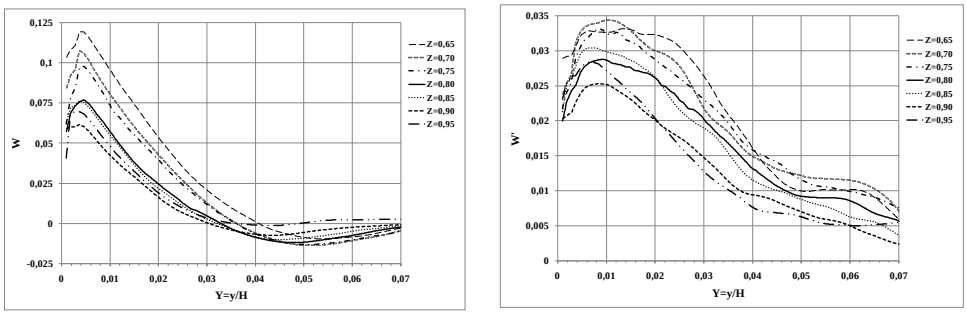

(a) ***(b)***

Dimensionless vertical component of the velocity (a) and his fluctuation (b) in the hot boundary layer

Figure 5 :

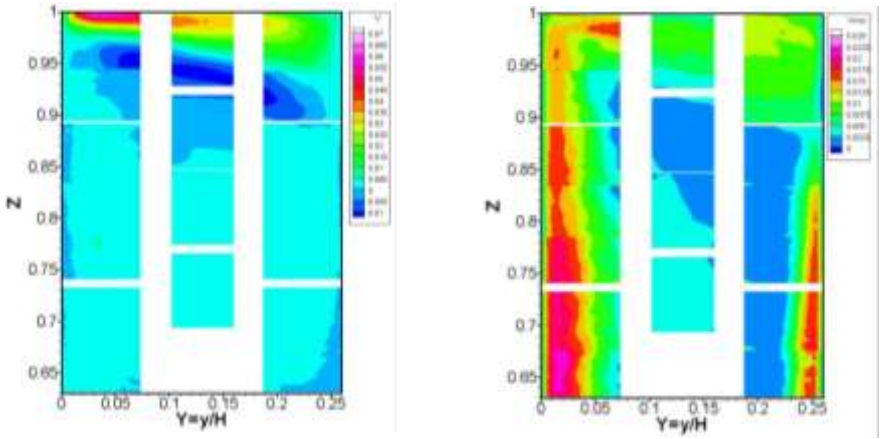

Mapping of horizontal component of the dimensionless mean velocity and its RMS fluctuation for Ra_H =1,2×10^{11}

The root mean square of velocity components was used to estimate 2D turbulent kinetic energy as follows:

$$k = \frac{\left(\overline{v'^2}+\overline{w'^2}\right)}{2} \qquad (1)$$

ISSN: 2277-9655
Impact Factor: 4.116
CODEN: IJESS7

Figure 6 :

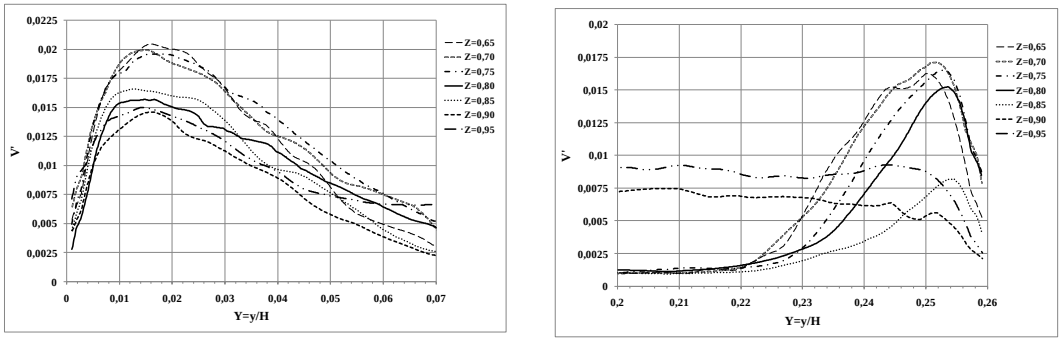

(a) **(b)**

Dimensionless horizontal component of the velocity fluctuation in the hot (a) and cold (b) boundary layers

A mapping of the 2D turbulent kinetic energy is represented on the **Fig. 7** which shows that the turbulent kinetic energy is concentrated in the boundary layers. The turbulent kinetic energy peaked near the hot wall ($0{,}63 \leq Z \leq 0{,}77$ et $0{,}01 \leq Y \leq 0{,}02$) at ~$4\times10^{-3}$ m^2/s^2. This area coincides with the region where the velocity becomes maximum for each height. The turbulent kinetic energy decreases to almost nothing outside the boundary layer.

Figure 7 :

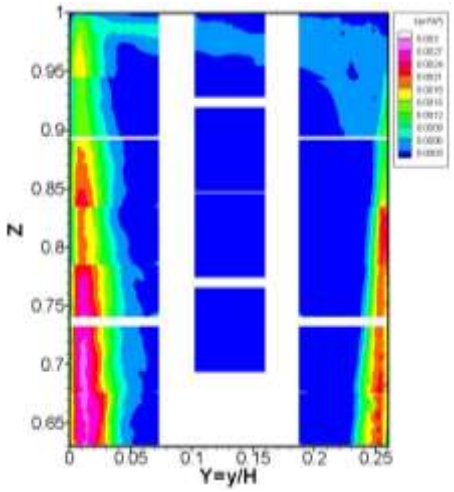

Mapping of turbulent kinetic energy for $Ra_H = 1{,}2\times10^{11}$.

III.1.2. Turbulence intensity

The dynamic turbulence intensity has been calculated in the boundary layer to 4cm from the hot wall ($Y \approx 0.01$) (location where the vertical velocity is maximum in the boundary layer) at different heights. This parameter has been also recorded to 4 cm from the ceiling ($Z \approx 0.99$) at different locations from the hot wall. The experimental results shown in **Fig. 8** are respectively based on the following equations:

$$I_w = \frac{\sqrt{\overline{(w')^2}}}{\overline{W}} \qquad (2)$$

$$I_v = \frac{\sqrt{\overline{(v')^2}}}{\overline{V}} \qquad (3)$$

According to the **Fig. 8a,** turbulence intensity decreases along the direction of the flow on isothermal walls, from Z=0.70 to 0.90. We found to the location Z=0.70 the turbulence intensity maximum of 28%. Along the horizontal flow direction near the ceiling, we are also recorded high turbulence intensity of about 24% (**Fig. 8b**) to the location Y= 0.06 from the hot wall. Indeed, the interaction between the main flow and the secondary flow near the ceiling which generates a shear zone, could explain this high level of turbulence.

ISSN: 2277-9655
Impact Factor: 4.116
CODEN: IJESS7

Figure 8 :

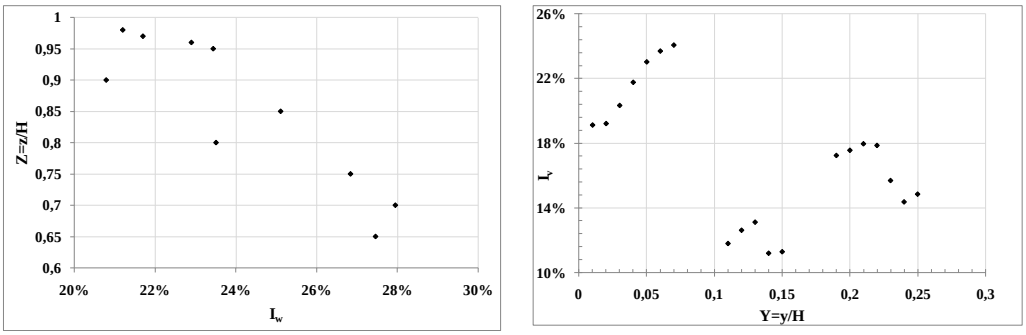

(a) **(b)**

Turbulence intensity in the boundary layer I_w (a) and near the ceiling I_v (b) for $Ra_H = 1.2\times10^{11}$.

III.1.3. Identification of vortex structures

One of the advantages of the PIV, is to allow near-instantaneous visualization of the flow through a wide enough field. This offers the possibility to see form and evolve vortex structures due to the turbulence flow. After image processing and validation of vectors by the Flowmanager software [15], several methods can be selected to highlight the vortices in the instantaneous velocity fields. However, this criterion has the major drawback of not distinguishing between vorticity and shear [17]. In this study, we used two methods called Q and λ2 criteria.

-*Criterion Q*: proposed by Hunt et al [18], it defines the vortices as being the area where the flow is dominated by the rotation tensor. Therefore, Vortex structures are identified by a representation of positive iso-values of Q while their centers are identified by the maximum values of Q.

-*Criterion λ2*: proposed by Jeong and Hussain [19], it is to look for the specific values. The areas to own negative values correspond to regions with minimum local pressure due to the whirling motion.

The center of vortex is identified by the extremum of the λ2 function.

By applying these criteria to a few fields of instantaneous velocity as the one represented in **Fig. 9**, we observed the vortex structures in the hot boundary layer which are highlighted by the λ_2 and Q criteria represented on **Fig. 10**. We have thus been able to identify in the vertical boundary layers, and on the outer edge of the hot boundary layer, the elliptical vortices having clockwise or anti-clockwise rotation (**Fig. 9**). It is found on the edge of the hot boundary layer that the vortex motion causes an ejection of hot air toward the core region of the cavity. This hot fluid is replaced by air less hot which is then driven by the main flow. Furthermore the presence of vortex structures causes a variation in the thickness of the hot boundary layer. This justifies the atypical behavior of the thickness of the boundary layer along the hot wall presented in [2].

Figure 9 :

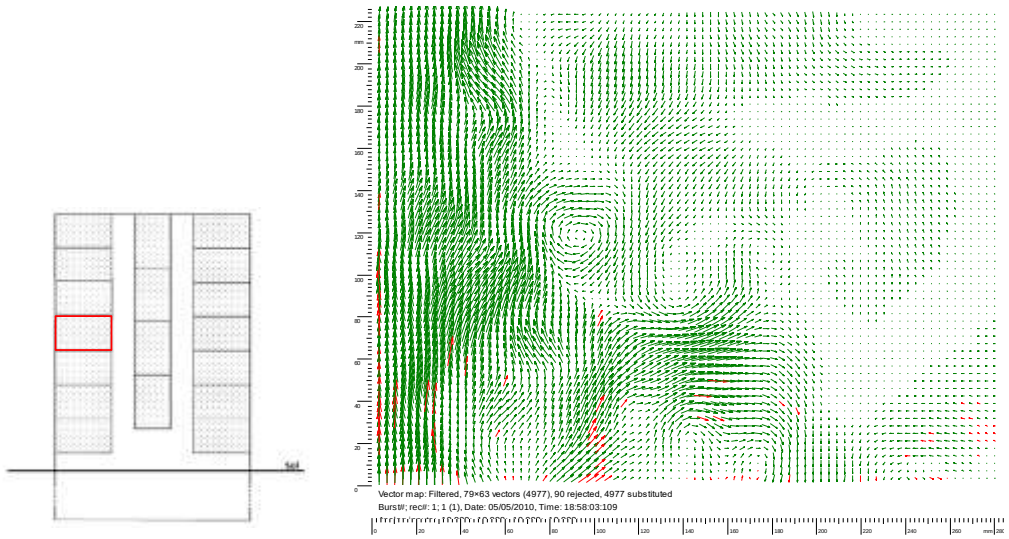

Field of instantaneous velocity along the hot wall ($0,790 \le Z \le 0,836$ and $0 \le Y \le 0,07$), $Ra_H = 1.2\times10^{11}$.

ISSN: 2277-9655
Impact Factor: 4.116
CODEN: IJESS7

Figure 10 :

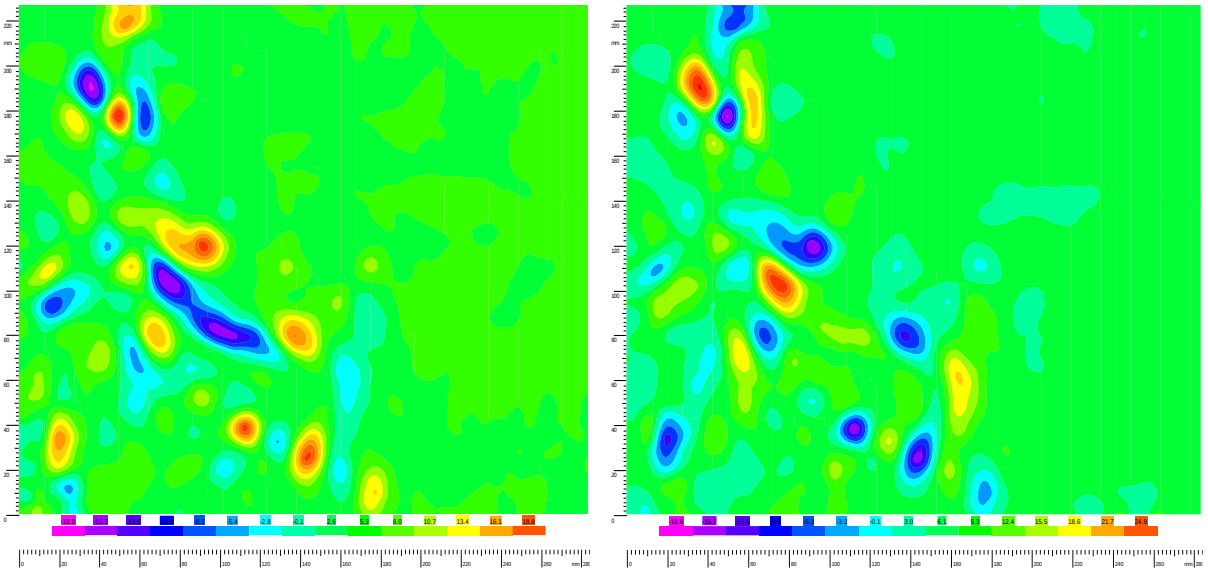

Detection of singular structures with Q (left) and λ2 (right) criteria (0.790 ≤ Z ≤ 0,836 and 0 ≤ Y ≤ 0.07), $Ra_H = 1.2\times10^{11}$.

Note that these measurements of large fields (20 ×30 cm^2) and the acquisition frequency of 4 Hz, unfortunately did not permit to do a spatio-temporal analysis of vortex structures.

III.2 Turbulent thermal parameters for $Ra_H = 1.2\times10^{11}$

III.2.1. The maximum of temperature fluctuation

The maximum of temperature fluctuation in the boundary layers was recorded at different heights (**Fig. 11**). The total temperature difference in the cavity is 20K and the temperature fluctuation can reach 2K at the location Z=0.30, corresponding to a thermal turbulence intensity in the order of 10 %.

It is also noted (**Fig. 11**) that for the region 0.20 < Z < 0.30 ($1\times10^9 < Ra_z < 3\times10^9$) is characterized by an amplification of disturbances probably due to the transition to turbulence.

Figure 11 :

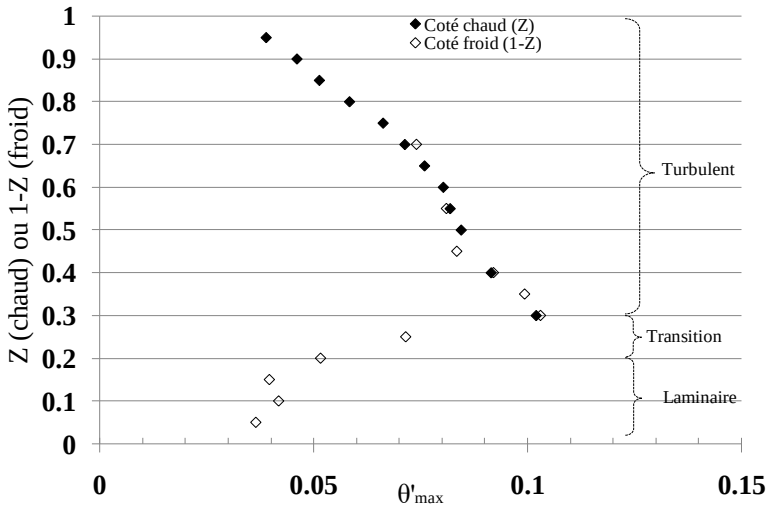

Maximum of the RMS value of temperature fluctuation in the hot boundary layer (to 7 mm from the hot wall) depending on the altitude for Rayleigh number equal to $1,2\times10^{11}$.

It is found on the table 1 and **Fig. 12** that whatever the temperature difference, the maximum RMS fluctuation seems to be constant and the position of the maximum of temperature fluctuation in the hot boundary

ISSN: 2277-9655
Impact Factor: 4.116
CODEN: IJESS7

layer is located in the area of transition from laminar to turbulence flow.

Table 1. Position of the maximum of temperature fluctuations de depending on the Rayleigh number.

Ra_H	θ'_{max}	Position de θ'_{max}(Z=z/H)	Ra(z)
$1,2\times10^{11}$	0,103	0,32	$3,77\times10^{9}$
$8,1\times10^{10}$	0,101	0,35	$3,45\times10^{9}$
$4,0\times10^{10}$	0,107	0,45	$3,67\times10^{9}$

Figure 12 :

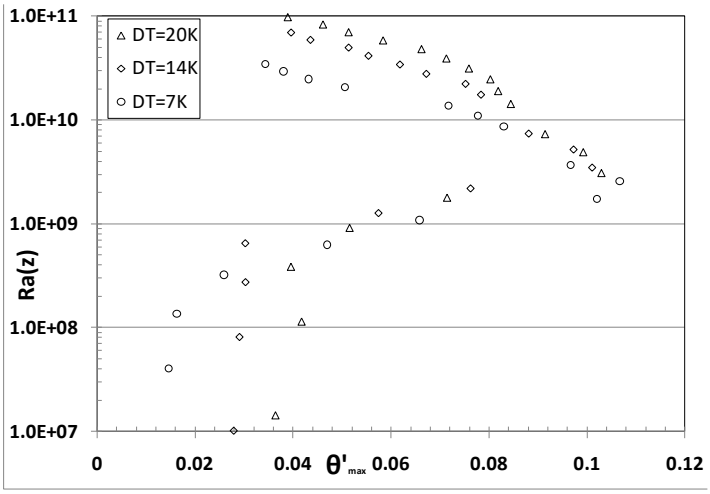

Evolution of the maximum of temperature fluctuations (RMS) with the height of cavity for different temperature.

III.2.2. The power spectral density (PSD)

The study of the transient behavior can provide valuable information on the occurrence or not of physical phenomena in a system [11]. The power spectral density (PSD) was obtained by using the fast Fourier transfer analysis of temperature fluctuations. The PSD expresses the distribution of power of the signal and can be used to investigate the transition from laminar to turbulent flow [13]. We then looked at the pace of the temporal signal of two regions, the core of the cavity and the vertical boundary layers. We have chosen 1024 samples and a sampling frequency of 10Hz for a duration of acquisition of 102.4 seconds either then a frequency resolution of 9.76 × 10-3Hz on a range of (0 ; 5 Hz).

III.2.2.1. Power Spectral Density in the core of the cavity

The recorded temperature fluctuation signal at the core region and the corresponding PSD as a function of frequency are shown in **Fig. 13**. It is clearly observed that temperature fluctuation in this region oscillate around the mean horizontal profile. Since the cavity core remains well stratified [1], this phenomenon can be attributed to internal waves. The fundamental frequency of these internal waves is $f = \frac{f_{bv}}{\sqrt{1+A_v^{-2}}}$ where f_{bv} is $\mathrm{Brunt} - \mathrm{Väisälä}$ frequency defined by $f_{bv} = \frac{1}{2\pi}\left(g\beta S\frac{\Delta T}{H}\right)^{1/2}$.

We recorded in the core region a fundamental frequency of 0.046 Hz very close of the theoretically frequency estimated of 0.05 Hz in this case.

III.2.2.2. Power Spectral Density in the boundary layers

The temperature fluctuation θ' (or θ_{rms}) at different locations near the hot and cold wall and the corresponding PSD as a function of frequency are shown in Fig. 14. One obvious feature is the peaks of the temperature signals. In the 1024 temperature points (in 102.4 s) of the time serial, the amplitudes of the peaks are not symmetric. This causes the time average temperature θ and the rms value of the temperature fluctuation, θ' (or θ_{rms}), to be unsteady. The shorter the time serial data, the more unsteady the θ and θ_{rms} values appear. The results exhibit the discontinuity in frequency which is one of the features of a turbulence flow. In laminar flow there is no

ISSN: 2277-9655
Impact Factor: 4.116
CODEN: IJESS7

physical parameter fluctuation and in a fully developed turbulent flow the fluctuation frequencies should be continuous.

Figure 13 :

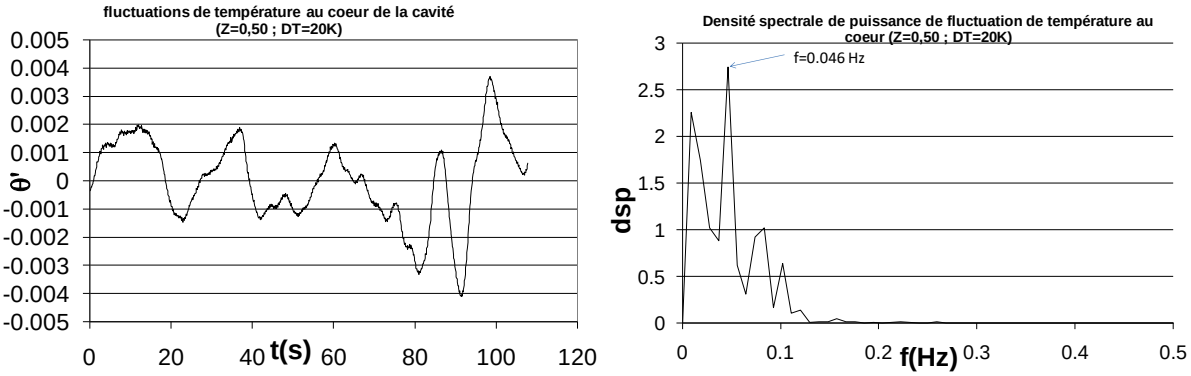

Signal of température fluctuation to the core (left) and Spectral power density associated (right)

- *In the hot boundary layer*

We present in **Fig. 14** the signal of temperature fluctuation in the hot boundary layer for two specific positions: to y =7 mm approximately from the hot wall which corresponds to the location of the maximum of velocity and of RMS fluctuation of temperature and output of the boundary layer thermal located about at y = 5cm (Y = 0,013) from the hot wall.

We note that the fluctuation of instantaneous temperature in the hot boundary layer reachs 4°C ($\theta' = T/\Delta T \approx 0.20$) at Z=0.55. According to this result, we found an intensity of thermal turbulence of 20 %.

The external border of the hot boundary layer remains disrupted, particularly in the upper half of the cavity. We recorded the temperature fluctuation of 2°C at the side Z=0.70, that corresponds to an intensity of thermal turbulence of 10 %. In effect, the main flow "return" (downflow) observed at the edge of the hot boundary layer, generates a strong shear, which induces significant temperature fluctuations as we have noticed earlier on the profiles of RMS fluctuations [2] (presence of a peak / tray in output of thermal boundary layer). For Y=0.013, we find also the asymmetry observed on the skewness factor [2].

Figure 14 :

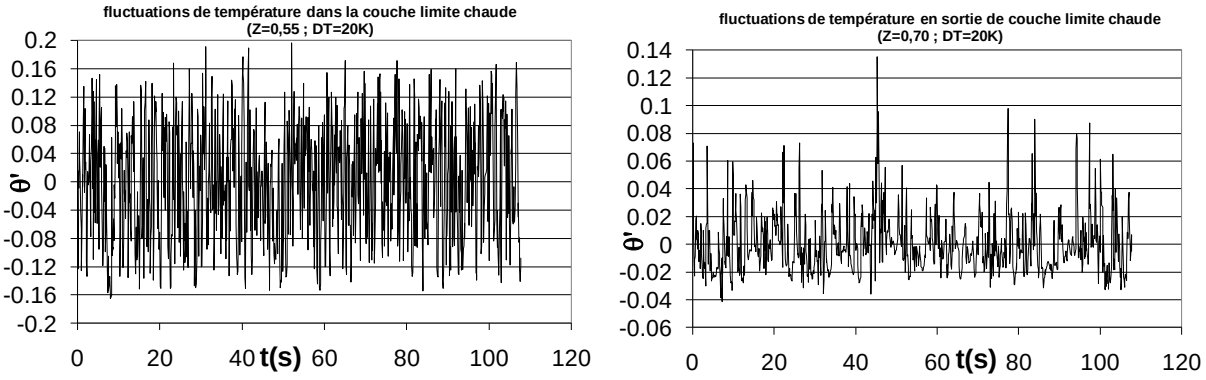

Time evolution of temperature fluctuations in the hot boundary layer (Y ≈ 0,0018) and on the edge of hot boundary layer (Y ≈ 0,013) for Rayleigh number equal to $1{,}2\times10^{11}$.

We present a few spectra of temperature fluctuation on the **Fig. 15**. There are several peaks in the PSD distributions whose number depends on the turbulence intensity; more intense fluctuation results in more peaks, making it fairly complex and the analysis of emerging frequencies. The results exhibit the discontinuity in frequency which is one of the features of a turbulence flow. In laminar flow there is no physical parameter fluctuation and in a fully developed turbulent flow the fluctuation frequencies should be continuous. However we found in the hot boundary layer (to 7 mm from the hot wall) a frequency of 1Hz which corresponds to the periodic oscillations in the form of Tollmien-Schlichting waves. We notice here that the measures of velocity by LDV

ISSN: 2277-9655
Impact Factor: 4.116
CODEN: IJESS7

carried out by N. ROUGER [20] had already helped to identify this type of instabilities.

Figure 15 :

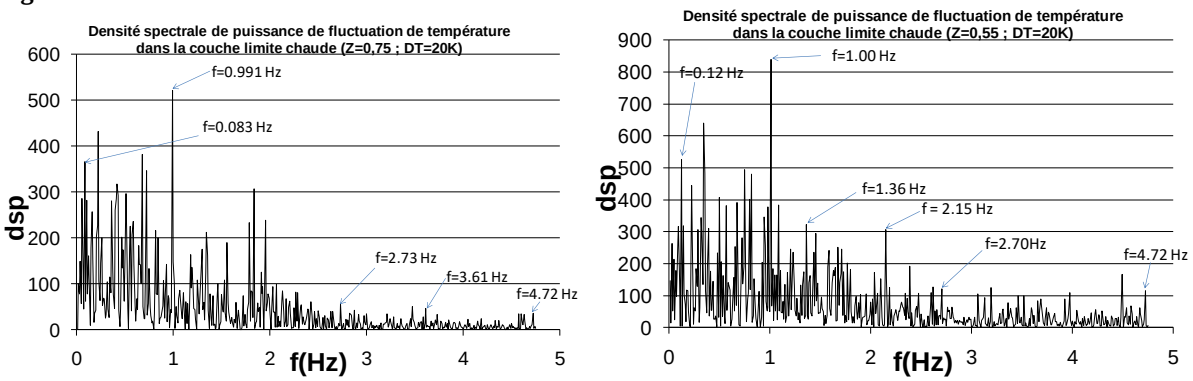

Spectral power density of température fluctuation in the boundary layer (Y ≈ 0,0018 i.e y = 7 mm from the hot wall) for Rayleigh number equal to 1,2×10^{11}.

We recorded, near the hot wall (to 0.7 mm from the hot wall), the higher frequencies (up to 4.72 Hz probably due to the large eddies ejected from the vertical hot boundary layer (**Fig. 15**).

At the outer edge of the hot boundary layer (about 5cm to the hot wall) it seems that a low frequency of 0.037 Hz dominates the fluctuation (**Fig. 16**). we conclude that eddies ejected from the vertical boundary layers at the hot upper region are large enough, to be characterised by excitation frequencies smaller than the Brunt-Väisälä frequency and maintain an internal wave of motion.

Figure 16 :

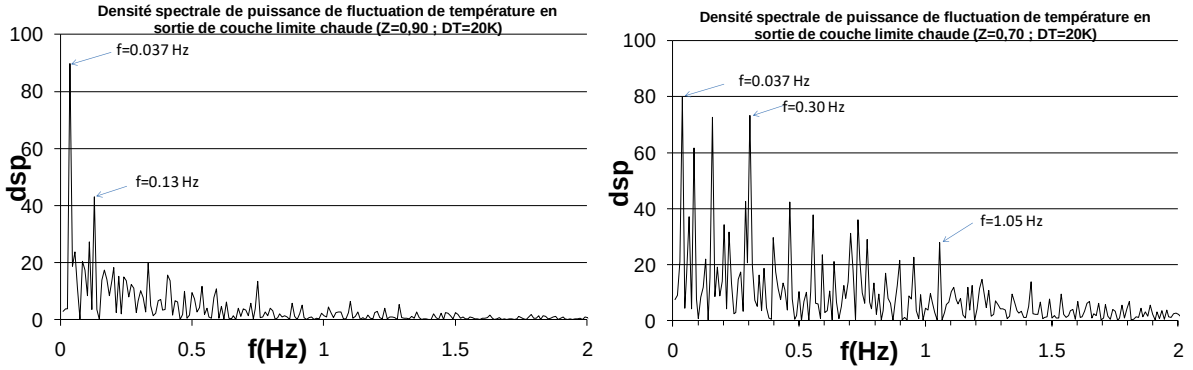

Spectral power density of temperature fluctuation at the edge of boundary layer (Y ≈ 0,013 i.e. y = 5cm from the hot wall) for Rayleigh number equal to 1,2×10^{11}.

A presentation of spectra in logarithmic scale at a distance of 7 mm from the warm wall is given on **Fig. 17**. We note that logically the spectra are more energy in the boundary layer than outside it (approximately a decade of more). In addition, on the spectra obtained, we found that from 1 Hz, the decay of the spectrum follows a law in f $^{-3}$ in the boundary layer and f $^{-5/3}$ is outside of the boundary layer. There is a decay already observed [21], characteristic of turbulent flows of natural convection or thermal gradients are important and therefore the forces of thrust of Archimedes are dominated [22]. We must also point out that the same kind of decay had already been observed, on the spectra of velocity. In effect, this result confirms the observations of Lumley [23]. According to Gebhart and al [24], the decay of the spectrum in the inertial box can take two values characteristics:

- a slope -5/3 [25] in the Inertial area, in external part of the boundary layer.
- a slope -3 ([23], [26]) in the Inertial zone in the presence of important buoyancy forces.

This slope (-3) is the result of the cascade energy when the Inertial area is affected by buoyancy effects of turbulent production. The regime of developed turbulence is reached (slope -3 spectral energy to higher frequencies), even if the spectra are rather of type line spectrum, indicating the survival of coherent structures in the boundary layers. We note in addition, that the more important peak is reached to the side Z=0.65 and corresponds to f=0.55 Hz of the same order of magnitude as the reference frequency considered for boundary layer flows, either $f_0 = \frac{a}{H^2} Ra^{1/2}$ = 0,5 Hz [11].

ISSN: 2277-9655
Impact Factor: 4.116
CODEN: IJESS7

Figure 17 :

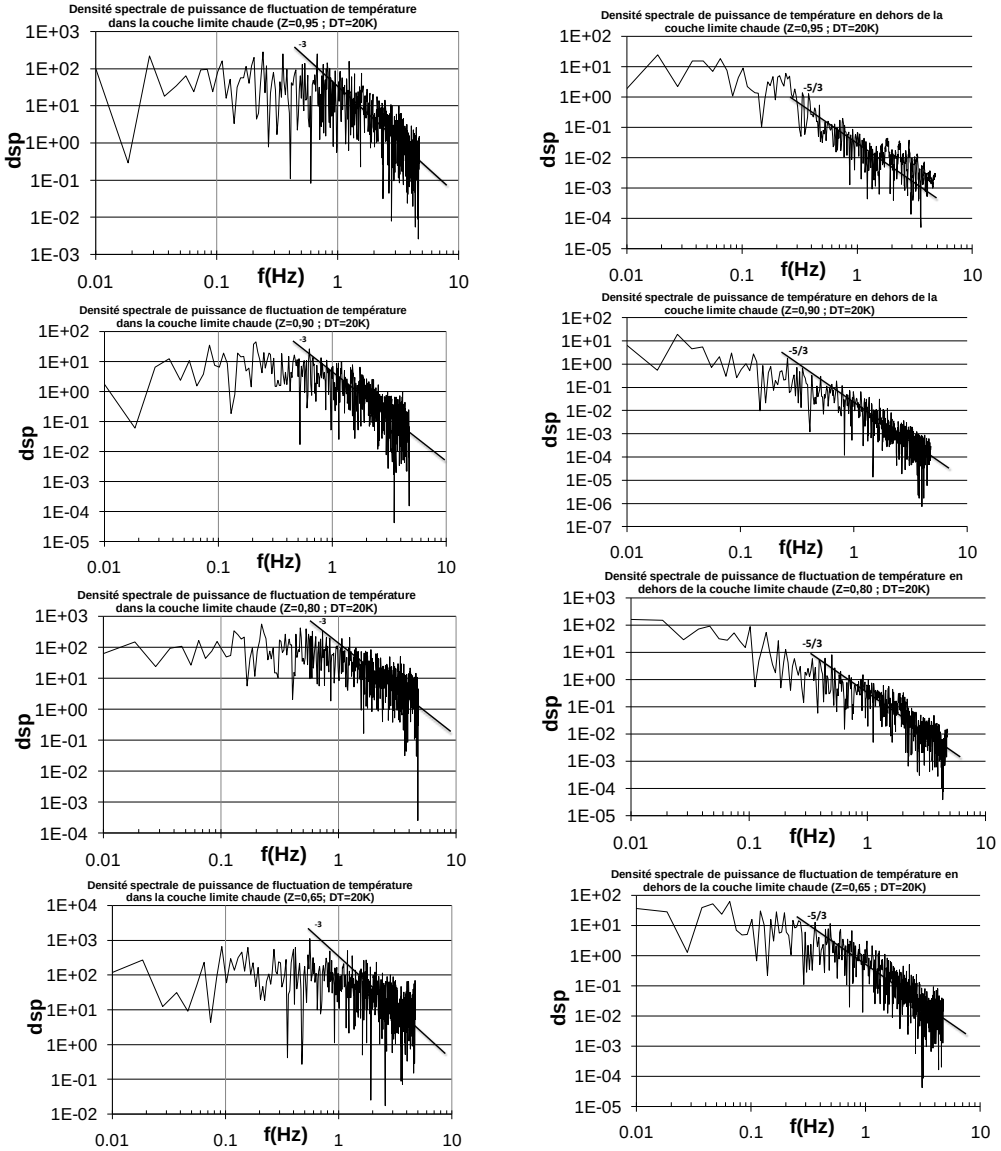

PSD in the hot boundary layer (Y ≈ 0,0018 left) and outside of the hot boundary layer (Y ≈ 0,052 right) for Rayleigh number equal to 1,2×10^{11} and 0,55 ≤ Z ≤ 0,70.

- *In the cold boundary layer*

We present in **Fig. 18** the temperature fluctuations in the boundary layer at y =7 mm to the cold wall, that corresponds to the location of the maximum of RMS fluctuation We find that the fluctuations in the cold boundary layer are relatively more important than in the hot boundary layer, reaching 5.4 °C to Z=0.75 . It is reported a discontinuous evolution of the temperature signal at this altitude.

ISSN: 2277-9655
Impact Factor: 4.116
CODEN: IJESS7

Figure 18 :

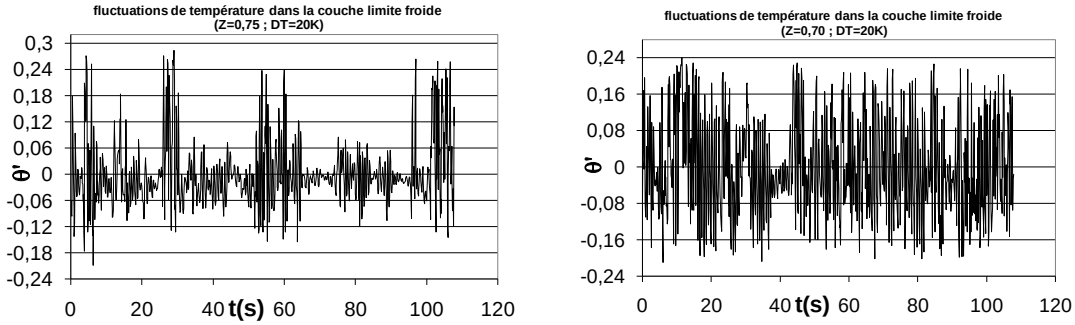

Time evolution of temperature fluctuations in the cold boundary layer for Rayleigh number equal to 1,2×10^{11} (from Y = $\frac{y}{H} \approx$ 0,0018 to the cold wall).

We represent on the **Fig. 19**, a few spectra in the cold boundary layer. For 0.85 < Z < 0.95 , the spectrum highlights a single low-frequency characteristic, and it is also noted that there are relatively many fewer peaks, which is evidence of the weak fluctuations within the boundary layer in this region. In the region 0.55 < Z < 0.80, we observed a signal fairly complex with the presence of several peaks, up to 4.5 Hz. The importance of fluctuations attests to a fully-developed turbulence in the boundary layer.

Figure 19 :

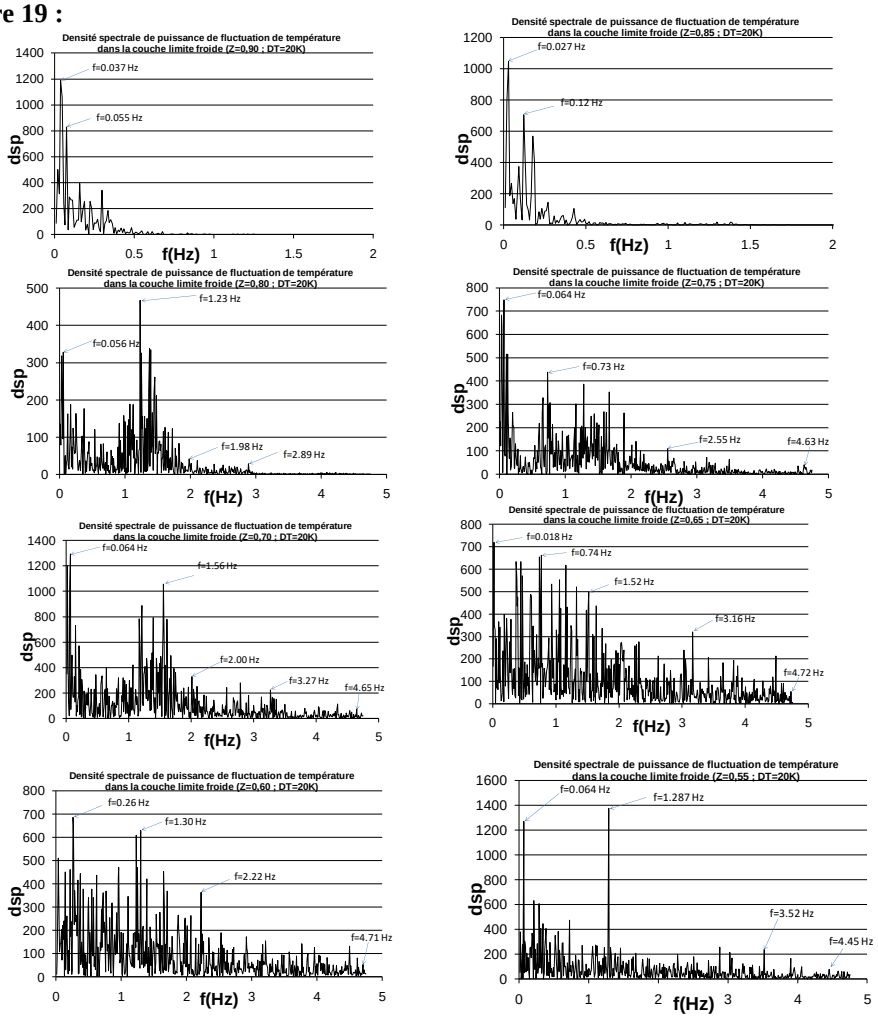

PSD of the temperature fluctuation in the cold boundary layer for Rayleigh number equal to 1,2×10^{11} (0,55 ≤ Z ≤ 0,95 ;

ISSN: 2277-9655
Impact Factor: 4.116
CODEN: IJESS7

to Y = $\frac{y}{H}$ ≈ 0,0018 from the cold wall).

At the outer edge of the cold boundary layer (**Fig. 20**), on the upper half of the cavity, there is a low frequency dominating between 0.027 Hz and 0.074 Hz, showing the existence of oscillations related to the internal waves.

Figure 20 :

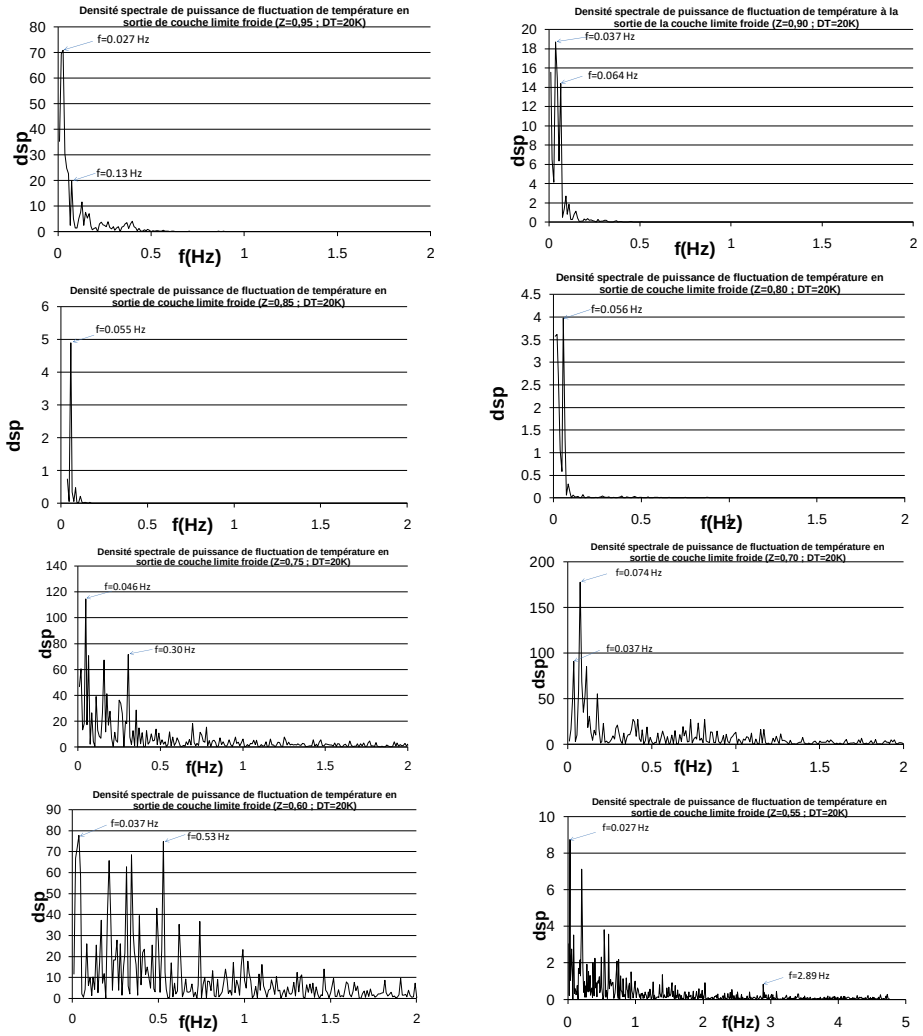

PSD of the temperature fluctuation in edge of the cold boundary layer for Rayleigh number equal to 1,2×10^{11} (0,55 ≤ Z ≤ 0,95 ; to Y = $\frac{y}{H}$ ≈ 0,013 from the cold wall).

IV. CONCLUSION

Our investigations have highlighted the character fully turbulent flow in the cavity with a turbulence rates approaching 30% and this, for the three configurations discussed. In addition, it has been observed that the "turbulence" is moving to the wall when the altitude increases. The PIV offers the advantage that it allows access to fields of instantaneous velocity; we have thus been able detect and monitor the development of coherent structures in the cavity using the criteria Q and λ2.

In a second time, we explored the boundary layers along the active walls and the court from the cavity. The analysis of our measures indicates thermal boundary layers very turbulent and relatively thick (approximately 5 cm). A spectral analysis of these measures has highlighted the presence of the frequency of Brunt-Väisälä who translated the oscillations of the court from the cavity. In addition it was noted in near wall, and in the output thermal boundary layer, the presence of frequencies of the order of the Hertz characterizing the presence of Tollmien-Schlichting waves. The frequency analysis has also revealed that the decay of the spectrum in the thermal boundary layers is

done in f^{-3}. This outcome was predictable because in the natural convection flow, the decay of the spectrum in f^{-3} is present in the areas where the forces of thrust of Archimedes exist, which is the case in the thermal boundary layers in natural convection. Outside the boundary layers, a classic slope -5/3 is found in the inertial area ([25], [26]).

V. REFERENCES

[1] Didier Saury, Nicolas Rouger, Francis Djanna, François Penot, Natural convection in an air-filled cavity: Experimental results at large Rayleigh numbers, International Communications in Heat and Mass Transfer, vol.38, Issue 6 (2011), 679-687.
[2] P. Belleoud, D. Saury, P. Joubert, D. Lemonnier, F. Djanna, Experimental investigations in an air-filled differentially-heated cavity at a large Rayleigh Numbers, Journal of Physics: Conference Series, 6th European Thermal Sciences Conférence (Eurotherm 2012), 395 (2012)012119.
[3] P.W. Giel, F.W. Schmidt, An experimental study of high Rayleigh number natural convection in an enclosure, in*: Proc. 8th. Int. Heat Transfer Conf.*, San Francisco, USA (1986) vol. 4, 1459-1464.
[4] R. Cheesewright, K.J. King, S. Ziai, Experimental data for the validation of computer codes for the prediction of two-dimensional buoyant cavity flows, *Winter Annual Meeting of ASME HTD* (1986) vol 60 75-82,
[5] R. Cheesewright, S. Ziai, Distributions of temperature and local heat-transfer rate in turbulent natural convection in a large rectangular cavity, in: *Proc. 8th. Int. Heat Transfer Conf.*, San Francisco, USA (1986) 1465-1470.
[6] R. Cheesewright, Natural convection from a plane, vertical surface in non-isothermal surroundings, *Int. J. Heat Mass Trans.* (1967) 10 1847-1859.
[7] P.L. Betts, A.A. Dafa'Alla, Turbulent buoyant air flow in a tall rectangular cavity, Winter Annular of ASME HTD (1986) 83-92.
[8] P.L. Betts, I.H. Bokhari, New experiments on turbulent natural convection of air in a tall cavity, in: Proc. 4th UK Heat Transfer Conference, (1995) 213-216.
[9] A. M. Lankhorst, Laminar and turbulent natural convection in cavities: modelling and experimental validation, PhD thesis, Technology University of Delft, Netherlands, (1991).
[10] A.M. Lankhorst, D. Angirasa, C.J. Hoogendoorn, LDV measurements of buoyancy induced flows in an enclosure at high Rayleigh numbers. Experimental Thermal and fluid science, (1993) vol 6, 74-79.
[11] S. Mergui et F. Penot. Natural convection in a differentially heated square cavity: experimental investigation at Ra=1.69×109, Int. J. Heat Mass Transfer, (1996) Vol. 39, 563-574.
[12] Y.S. Tian, T.G. Karayiannis, Low turbulence natural convection in an air filled square cavity. Part I : the thermal and fluid flow fields. International Journal of Heat and Mass Transfer, (2000) vol 43, 849-866.
[13] Y.S. Tian, T.G. Karayiannis, Low turbulence natural convection in an air filled square cavity. Part II : the turbulence quantities. International Journal of Heat and Mass Transfer, (2000) vol 43, 867-884.
[14] F. Ampofo, T.G. Karayiannis, Experimental benchmark data for turbulent natural convection in an air filled square cavity, International Journal of Heat and Mass Transfer, (2003) vol 46 (19) 3551-3572.
[15] Dynamic Studio software and Introduction to PIV Instrumentation, Dantec, Dynamics GmbH, (2000) Publication number: 9040U3625.
[16] J. Salat. Contribution à l'étude de la convection naturelle tridimensionnelle en cavité différentiellement chauffée. Thèse de Doctorat de l'Université de Poitiers (2004).
[17] O. Skurtys, Contribution au contrôle de la convection naturelle par excitation thermique des couches limites en cavité différentiellement chauffée. Thèse de Doctorat de l'Université de Poitiers, (2004).
[18] J. C. R. Hunt, A.A. Wray, and P. Moin. Eddies, stream and convergence zones in turbulent flows. Tech. Report CTR-S88, Center for Turbulence Research, (1988).
[19] Jeong and F. Hussain, « On the identification of a vortex », J. Fluid Mech., (1995) vol 285 69–94.
[20] N. Rouger, Sensibilité de la convection naturelle en cavité différentiellement chauffée à des variations de paramètres géométriques, thermiques et massiques. Thèse de Doctorat de l'Université de Poitiers, 2009.
[21] D. Saury, N. Rouger, F. Djanna, F. Penot, Caractérisation des écoulements de convection naturelle turbulente à grand nombre de Rayleigh. Congrès Francophone des Techniques Laser, CFTL 2008, Futuroscope, 16-19 Septembre 2008, pp. 167-174, ISBN 2-905267-62-3.
[22] M. Okamoto, Theoretical Investigation of Energy and Thermal Intensity Spectra in Buoyancy-DrivenTurbulent Flows, J. Phys. Soc. Jpn., 65, pp.3193-3201, 1996.

[23] J. L. Lumley, Interpretation of time spectra measured in high-intensity shear flows. Phys. Of Fluids, Vol 8, pp1056-1062,1965.
[24] B. Gebhart, Y. Jaluria, R. L. Mahajan, B. Sammakia, Buoyancy-induced flows and transport, reference edition, Springer-Verlag, Berlin,1988.
[25] S. Corrsin, On the spectrum of isotropic temperature fluctuations in an isotropic turbulence. J. appl. Phys., 22, pp 469-473, 1951.
[26] G. N. Shur, Eksperimental'nyye issledovania energeticheskogo spectra atmosfernoy turbulentnosti. Tsentral' naya aerologicheskaya observatoriya. Trudy 43, 79-90, Trans. As AID Report T-63-55 Aerospace Info. Div., Lib. Cong., 1962.

CITE AN ARTICLE

FL, D. K., G, T. J., BE, M. F., D, S., P, J., & D, L. (2017). AN EXPERIMENTAL STUDY OF TURBULENT NATURAL CONVECTION IN AN AIR FILLED DIFFERENTIALLY HEATED CAVITY: THE TURBULENCE QUANTITIES . *INTERNATIONAL JOURNAL OF ENGINEERING SCIENCES & RESEARCH TECHNOLOGY*, *6*(9), 51-65. Retrieved September 5, 2017.